Progress In Electromagnetics Research M, Vol. 110, 25–38, 2022

Wavelet Denoising of Echo Signal of Unilateral Magnetic Resonance Sensor

Pan Guo[1, *], Chenjie Yang[1], Yunfeng Zhu[2], Jiamin Wu[3, 4], and Zheng Xu[2]

Abstract—Carr-Purcell-Meiboom-Gill (CPMG) is generally used as the measurement sequence of unilateral NMR (UMR) sensors, and the NMR signals collected by the sequence are composed of a series of echo signals. In the traditional CPMG measurement signal, each echo peak value is first taken and then denoised, which would lead to the inaccuracy of the peak point taken, resulting in deviation. To ensure the measurement result more accurate, this paper proposes to employ wavelet technology to denoise the echo signal first, and then take the peak point to analyze the data. Firstly, a simplified model of the spin-echo signal without the influence of gradient magnetic field was established, and white noise was applied to a certain extent. Then, Signal to Noise Ratio (SNR) and Root Mean Square Error (RMSE) were used as evaluation indexes. The denoising effects under different wavelet bases and thresholds were compared. Finally, the Matlab simulation result showed that wavelet analysis had a good effect on the denoising of unilateral NMR spin echo signal.

1. INTRODUCTION

Unilateral NMR is derived from the inside-out NMR technique [1], in which a wave spectrometer is placed in a good cavity to image the fluid surrounding the cavity. Similar devices are used for product quality testing and medical diagnostics, among other things [2–6]. Although the technique has been proposed for over 30 years, it was not until well logging companies began Zeeman splitting commercial research into nonuniform field techniques, and NMR-MOUSE equipment was developed that the technique was taken seriously by the NMR technology industry.

The raw data of a single-sided NMR measurement is a series of echo signals whose amplitude decays with time measured by an RF coil under the action of a CPMG pulse sequence, which is differentiated by analyzing the echo signals of different substances with different relaxation characteristics of hydrogen protons [7]. The traditional method of analyzing the single-sided NMR signal is to first take the peak points of the individual echo signals and to fit the signals consisting of the individual peak points to a multi-exponential fit using the inverse Laplace transform [8]. Currently, due to various factors such as magnetic field uniformity, coil sensitivity, and environmental noise, the actual measured unilateral NMR spin-echo signals contain a large amount of noise [9, 10], which requires noise reduction of the signal before further analysis.

In the field of signal analysis, signal noise reduction is one of the important research topics [11, 12]. There are many types of research on denoising methods of magnetic resonance signals [13–22]. Gerig and Kubler first proposed a multi-echo MRI image post-processing method based on AD filters [14] with higher spatial and spectral dimensions and demonstrated effective noise reduction and sharpening. Krissian and Aja-Fernandez proposed a new filtering method to remove Rician noise in MRI, namely

Received 8 February 2022, Accepted 14 March 2022, Scheduled 24 April 2022

* Corresponding author: Pan Guo (guopan@cqnu.edu.cn).

[1] College of Physics and Electronic Engineering, Chongqing Normal University, Chongqing, China. [2] State Key Laboratory of Power Transmission Equipment & System Security and New Technology, Chongqing University, Chongqing, China. [3] Shenzhen Academy of Aerospace Technology, Shenzhen, Guangdong, China. [4] Harbin Institute of Technology, Harbin, China.

matrix diffusion filters [15] to remove Rician noise. Pizurica et al. introduced wavelet-based filters that are also effective in removing noise from MRI images, which were filtered in the transform domain [16]. Principal Component Analysis (PCA), proposed by Muresan and Parks [17], and the Discrete Cosine Transform (DCT), proposed by Yaroslavsky et al. [18], have also been applied to the image noise reduction field. An information-theoretic approach using non-parametric density estimation to describe the neighborhood structure was proposed by Awate and Whitaker. The formulation can be easily generalized to simultaneous noise reduction for multimodal MRI and exploits the relationship between modes [19] to further improve performance. Manjón et al. exploit the sparsity and self-similarity of MR images for 3D noise reduction [20]. Convolutional neural networks (CNNs) are widely used in image restoration due to their strong discriminative power. Zhang et al. proposed a Denoising Convolutional Neural Network, (DnCNN) [21], which uses residual learning and Batch Normalisation (BN) to speed up the training process and improve denoising performance. Jiang et al. developed a Multi-Channel DnCNN (MCDnCNN) [22] method with two training strategies to remove noise from MR images with or without a specific noise level. The traditional signal denoising method uses Fourier transform to filter to suppress the high-frequency noise. However, for the unilateral NMR signal, its frequency domain characteristics are not obvious due to the influence of the complex phase and frequency distribution of the signal. Meanwhile, the signal attenuation is fast and shows non-periodicity, so the effect of this method is not obvious [23]. Wavelet Analysis (WA) is a branch of mathematics developed in the past 20 years, which is the result of the epoch-making development of Fourier analysis [24–27]. Since 1992, the theory and method of wavelet analysis have been successfully applied to the fields of smoothing and noise filtering, data compression, image processing, etc. of analytical chemical signals [28]. Compared with other denoising methods mentioned above, the advantage of wavelet analysis is mainly due to the following characteristics of wavelet transform: (1) Low entropy. The sparse distribution of wavelet coefficients reduces the entropy of the transformed image; (2) Multi-resolution property. Due to the multi-resolution method, the non-smooth characteristics of the signal can be very well portrayed; (3) De-correlation. Because the wavelet transform can de-correlate the signal, and the noise has a tendency to whiten after the transform, the wavelet domain is better than the time domain for noise removal; (4) Base selection flexibility. Since the wavelet transform can be flexible in choosing the basis, it can also choose multiple wavelets, wavelet packets, translational wavelets, etc. according to the signal characteristics and denoising requirements, and for different occasions, different wavelet mother functions can be chosen. Wavelet analysis has the above characteristics and is, therefore, suitable for the denoising of unilateral NMR spin echo signals.

2. FUNDAMENTAL

2.1. Mathematical Model of Spin-Echo Signals

Nuclear magnetic resonance (NMR) is a physical process in which an atomic nucleus with a non-zero magnetic moment undergoes Zeeman splitting of the spin energy level in the presence of an external magnetic field and resonates to absorb radiofrequency radiation of a certain frequency. Unlike medical imaging, unilateral MRI does not require spatial localization of the signal. Based on this principle, single-sided MRI equipment generally consists of a main magnet, a radiofrequency coil, and a spectrometer [29]. The main magnet provides a uniform main magnetic field B_0, under the action of which all hydrogen protons in the field point towards the same magnetic moment as B_0, while undergoing spin motion at the same frequency. This frequency is called the Larmor frequency (where γ is the spin-to-magnetic ratio of the nucleus):

$$\omega_0 = \gamma B_0 \tag{1}$$

The application of an RF pulse to a system of protons in a uniform field causes resonant absorption of the system, resulting in two effects: ① the protons jump from a lower to a higher energy level, and the longitudinal magnetization decreases from M_0 to M_z; ② the incoming protons are no longer uniformly distributed in the upper and lower cones but move at the same speed and in the same direction, i.e., in the same phase, resulting in transverse magnetization and transverse magnetization vector M_{xy}. Depending on the time and intensity of the applied RF pulse, the angle of θ changes accordingly, and

this relationship is expressed by the following equation:

$$\theta = \gamma B_1 \tau \tag{2}$$

where B_1 is the magnitude of the magnetic field in the RF pulse, and τ is the pulse action time. Depending on the θ angle of the pulse excitation, the RF pulse can be divided into 90° pulses, 180° pulses, and partially flipped pulses.

When the radio frequency pulse stops, two things happen accordingly: (i) protons of higher energy levels jump to lower energy levels; (ii) protons appear out of phase with each other. These two processes occur simultaneously but independently of each other. The first process is macroscopically manifested by a gradual recovery of the longitudinal magnetization intensity vector from M_z to M_0, and is known as the longitudinal relaxation process. The speed of this process depends on the interaction between the protons and their surroundings and can be expressed by the following equation [10]:

$$M_z(t) = M_0\left(1 - e^{\frac{-t}{T_1}}\right) \tag{3}$$

where T_1 is the longitudinal relaxation time, usually taken as the time required for M_Z to recover from 0 to $0.63M_0$. The second process is the gradual dispersion and eventual uniform distribution of protons from the same phase, which is macroscopically manifested by the decay of the transverse magnetization intensity vector M_{xy} from a maximum $M_{xy\max}$ to zero, and is known as the transverse relaxation process. This process depends on the proton spin-spin interaction but is susceptible to the inhomogeneity of the external magnetic field, and when the external field is uniform, the decay process is expressed as:

$$M_{xy}(t) = M_{xy\max} e^{-\frac{t}{T_2}} \tag{4}$$

where T_2 is the transverse relaxation time, usually taken as the time required for M_{xy} to decay from $M_{xy\max}$ to $0.37M_{xy\max}$. The transverse relaxation process and longitudinal relaxation process are carried out independently. By detecting the change process of the transverse magnetization vector and setting the pulse sequence reasonably, T_2-weighted detection, T_1-weighted detection and proton density-weighted detection can be achieved. To simplify the analysis, we use the signal generated by the spin-echo sequence (e.g., Figure 1) as the signal source for analysis and processing.

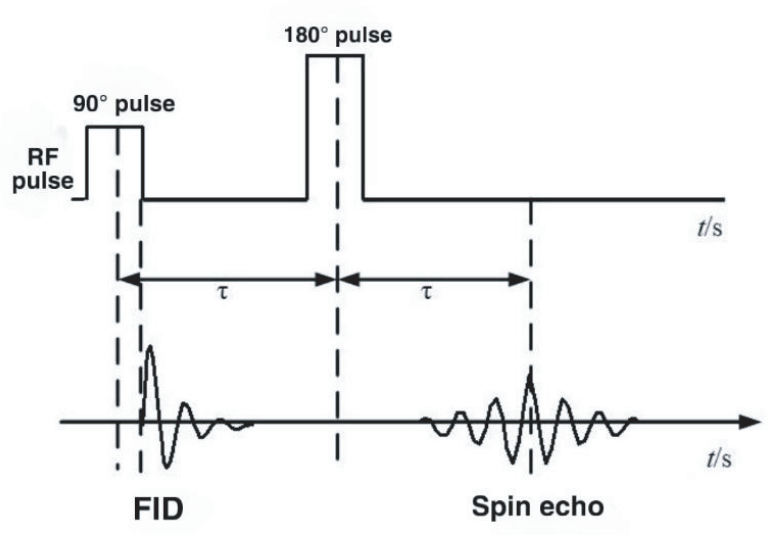

Figure 1. Spin-echo sequence.

A 90° pulse is first applied to flip the magnetic moment, and the transverse magnetization vector reaches a maximum. After the RF pulse stops, the nuclear magnetic moment is fed around the main magnetic field at the Larmor frequency ω_0, and the transverse magnetization vector decays in magnitude T_2. Afterward, the nuclear magnetic moment flips 180° under the action of the 180° pulse, and the

whole process is symmetrical, so that t_1=t_2, and the spin-echo signal is symmetrical to the left and right. According to the above analysis, taking the middle position of the spin-echo signal as the time origin, the spin-echo signal can be expressed as:

$$S(t) = \begin{cases} M_{xy\max} e^{\frac{t}{T_2}} * \cos(\omega_0 t) & (t < 0) \\ M_{xy\max} e^{\frac{-t}{T_2}} * \cos(\omega_0 t) & (t \geq 0) \end{cases} \tag{5}$$

where $M_{xy\max}$ depends on the proton density ρ of the substance to be detected. $\omega_0 = 8.5\,\text{MHz}$ in the general environment of a single-sided magnet with a magnetic field strength of 0.2 T.

2.2. Basic Principles of Wavelet Noise Reduction

The wavelet transform is a mathematical analysis method developed in recent years [27, 29] and is a development of the Fourier transform. The mathematical model of a one-dimensional noise-bearing signal is:

$$f(t) = S(t) + n(t) \tag{6}$$

where $n(t)$ is a Gaussian white noise obeying $N(0, \sigma^2)$. The basic principle of signal denoising using wavelets is that after wavelet decomposition, the coefficients with larger amplitudes contain important information about the signal, while those coefficients that are uniformly distributed and smaller in number and amplitude correspond to noise. Based on this principle, the signal can be reconstructed by decomposing the signal into multiple layers of wavelets, obtaining the detailed and approximate components, and processing the detailed coefficients according to a certain threshold.

The main steps of the whole denoising process are as follows:

1) Base Selection

Different wavelet bases have different properties and therefore have their specific trial environment, and different wavelet bases have different noise reduction results on the signal. The main properties of wavelet bases include tight branching, regularity, symmetry, completeness, and continuity. No wavelet can satisfy all these properties at the same time, so finding a suitable wavelet base is the first step in signal noise reduction.

2) Layer Selection

The number of wavelet decomposition layers is also one of the factors affecting the effectiveness of wavelet noise reduction. The theoretical maximum number of decomposition layers is $\log_2 N$. The larger the number of decomposition layers is, the more obvious the difference is between the noise characteristics and signal characteristics, i.e., the more obvious the noise reduction effect is, but at the same time it will also cause an increase in the reconstruction error, i.e., the distortion increases. It is also important to choose a reasonable number of decomposition layers.

3) Wavelet Decomposition

Wavelet decomposition is the core of the multi-resolution analysis. The commonly used wavelet decomposition algorithm is the famous Mallat decomposition algorithm, where each layer of decomposition yields two signals, approximate signal and detailed signal, and then the approximate signal can be decomposed in the next layer.

4) Threshold Processing

Hard thresholding (HT): sets wavelet coefficients with absolute values less than a given threshold to 0, while wavelet coefficients with absolute values greater than the threshold remain unchanged, i.e.:

$$w' = \begin{cases} w & |w| \geq T \\ 0 & |w| < T \end{cases} \tag{7}$$

Soft Thresholding (ST): sets wavelet coefficients with absolute values less than a given threshold to zero, while all wavelet coefficients with absolute values greater than the threshold are subtracted from the threshold, i.e.,

$$w' = \begin{cases} \operatorname{sgn}(w)(|w| - T) & |w| \geq T \\ 0 & |w| < T \end{cases} \tag{8}$$

where w is the wavelet coefficient, w' the thresholded wavelet coefficient, T the threshold value, and $T \geq 0$.

5) Wavelet Reconstruction

The thresholded detail signal and approximate signal generated by the decomposition are reconstructed to obtain the denoised signal. To judge the noise reduction performance of the reconstructed signal, we use the signal-to-noise ratio (SNR) and mean square error (RMSE) as evaluation metrics. The SNR is defined as (Here we define the unit of SNR as dB, where the numerator represents the effective power of the signal, and the denominator represents the effective power of the noise.):

$$SNR = 10 \lg \left(\frac{\sum_{i=1}^{N} S_i^2}{\sum_{i=1}^{N} (f_i - S_i)^2} \right) \tag{9}$$

The mean square error is defined as:

$$RMSE = \sqrt{\frac{1}{N} \sum_{i=1}^{N} (f_i - s_i)^2} \tag{10}$$

where S_i denotes the ith sample of the original signal; f_i denotes the ith sample of the denoised signal; and N is the total number of samples.

3. EXPERIMENTAL METHOD

Matlab was used to carry out the simulation experimental research, including the establishment of the spin-echo signal simulation model, the construction of signal-to-noise ratio and mean square error function, the use of different wavelet bases for noise reduction processing, and the use of different thresholds for noise reduction processing.

3.1. Simulation Model of Spin-Echo Signals

This paper focuses on the effect of wavelet analysis on the noise processing of spin-echo signals, making the following two assumptions for analytical convenience:

① Assume $\omega_0 = 100\,\text{Hz}$.

② Assume $M_{xy\max} = \rho$.

These two assumptions reduce the computational effort while maintaining the basic characteristics of the actual signal. According to Nyquist's theorem, the sampling frequency $\omega_s > 2\omega_0$ is taken here as $\omega_s = 1/1024$ for computational convenience.

Based on the above assumptions, we arbitrarily selected the composite signals from three tissues, namely, cerebral white matter, cerebral grey matter, and cerebrospinal fluid, as the signal sources [30]. According to Eq. (5), the mathematical expression of the original signal is:

$$s(t) = \begin{cases} \sum \rho_i * e^{\frac{t}{T_{2i}}} * \cos(\omega_0 t) & (t < 0) \\ \sum \rho_i * e^{-\frac{t}{T_{2i}}} * \cos(\omega_0 t) & (t \geq 0) \end{cases} \tag{11}$$

where ρ_i $(i = 1, 2, 3)$ indicates the proton density of white matter, grey matter, and cerebrospinal fluid, respectively, whose values are shown in Table 1; T_{2i} $(i = 1, 2, 3)$ indicates the lateral relaxation time of white matter, grey matter, and cerebrospinal fluid, respectively, whose values are shown in Table 1.

The following noise is applied to the original signal. The signal noise is mainly realized in two ways. One is the deviation n_i from ω_0 due to magnetic field inhomogeneity, and the other is the overall signal noise due to various equipment and environmental factors $\varepsilon(t)$. The mathematical expression for a signal containing noise is then:

$$S(t) = \begin{cases} \sum \rho_i * e^{\frac{t}{T_{2i}}} * \cos[(\omega_0 + n_i) t] + \varepsilon(t) & (t < 0) \\ \sum \rho_i * e^{\frac{-t}{T_{2i}}} * \cos[(\omega_0 + n_i) t] + \varepsilon(t) & (t \geq 0) \end{cases} \tag{12}$$

Table 1. Relaxation times of common tissues.

Tissues	T_1 (ms)			T_2 (ms)	Proton density (%)
	0.2 T	1.0 T	1.5 T		
Cerebral white matter	390	620	778	76	10.6
Cerebral gray matter	490	810	998	91	10.6
Cerebrospinal fluid	1400	2500	3000	140	10.8

where n_i is the white noise obeying $N(5, 1)$, and $\varepsilon(t)$ is the white noise with SNR = 2.

Based on the above analysis, we implemented the signal simulation on Matlab and obtained the curves of the original signal and noise-laden signal as shown in Figure 2.

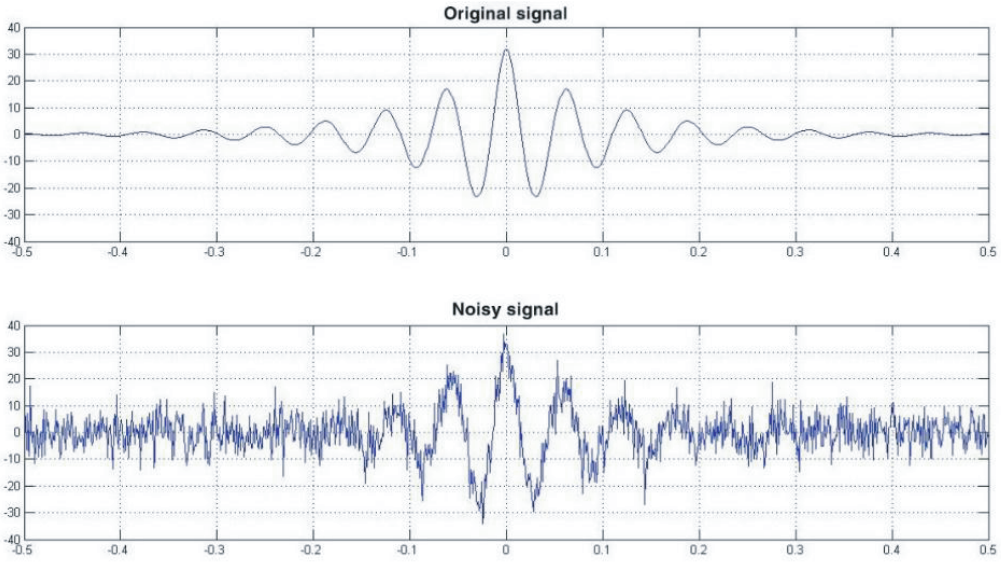

Figure 2. Original signal and noisy signal.

According to Eq. (9) and Eq. (10), the SNR of the spin-echo simulation signal is calculated by Matlab programming = 2.0806, RMSE = 5.6327.

3.2. Simulation Methods for Wavelet Noise Reduction

According to the analysis in Section 2.2, the quality of wavelet noise reduction depends on the choice of wavelet basis, the choice of decomposition layers, and the choice of threshold. This paper conducts comparative simulation experiments for these three aspects.

1. Different wavelet bases are used to perform different levels of noise reduction on the noise-containing signal. With 1024 sampling points, the maximum number of decomposition layers is 10. Here, we choose $N = 3, 4, 5, 6$ for comparison. For wavelet bases, we select the typical wavelet bases haar, db4, db6, sym4, sym6, coif2, coif4, bior3.9, bior6.8, rbio3.7, rbio6.8 commonly used for one-dimensional transforms. For the different levels and wavelet bases of decomposition, all detail components are set to 0 for reconstruction to eliminate the effect of thresholding, and thus comparing the values of SNR and RMSE for different wavelet bases and decomposition levels and analyzing them, this process was implemented using Matlab's wavelet function.

2. Noise reduction processing with different thresholds. For the data obtained from the previous experiment, the best three wavelet bases and decomposition layers were selected for the noise reduction process, comparing the noise reduction effects under soft and hard thresholds and different threshold sizes. This process is implemented using Matlab's wavelet menu function.

4. RESULT ANALYSIS

4.1. Noise Reduction Effect of Different Wavelet Bases and Decomposition Layers

Based on the above analysis, the wavedec() and waverec() functions are used to implement a comparison of the multi-layer decomposition of different wavelet bases. The simulation results are shown in Figure 3 to Figure 13.

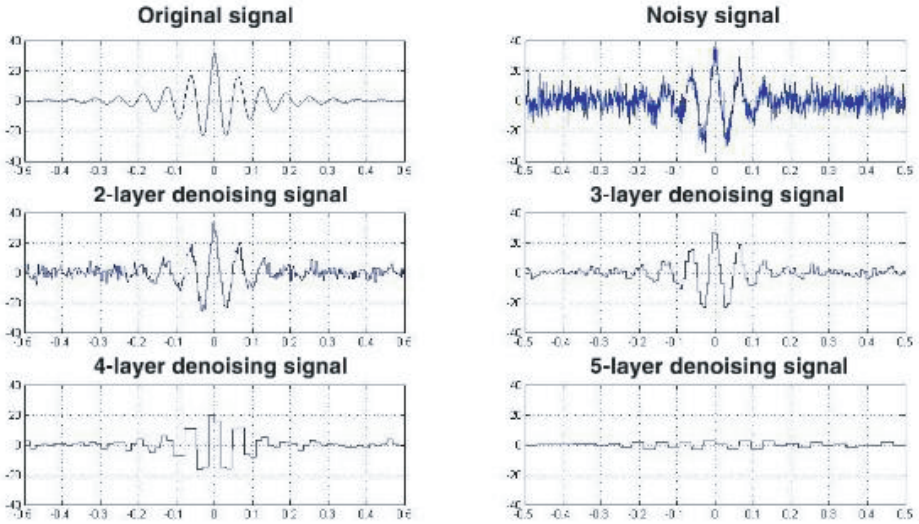

Figure 3. Noise reduction of haar wavelets.

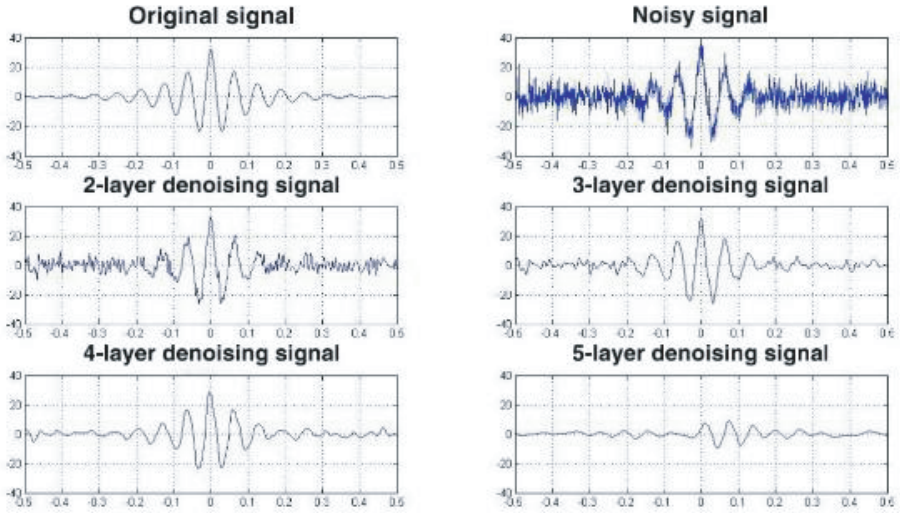

Figure 4. Noise reduction of db4 wavelets.

The signal-to-noise ratio and mean square error calculations for the various noise reduction processing modes are shown in Table 2.

From the graph of the reconstructed signal and the SNR and RMSE data, it can be seen that, except for db6, distortion occurs when $N > 4$, and with further 6-layer decomposition and reconstruction for db6 wavelet noise reduction, serious distortion occurs; therefore, N should not be taken as large. At the same time, the noise reduction effect at $N = 2$ is not obvious; therefore, for this spin-echo simulation

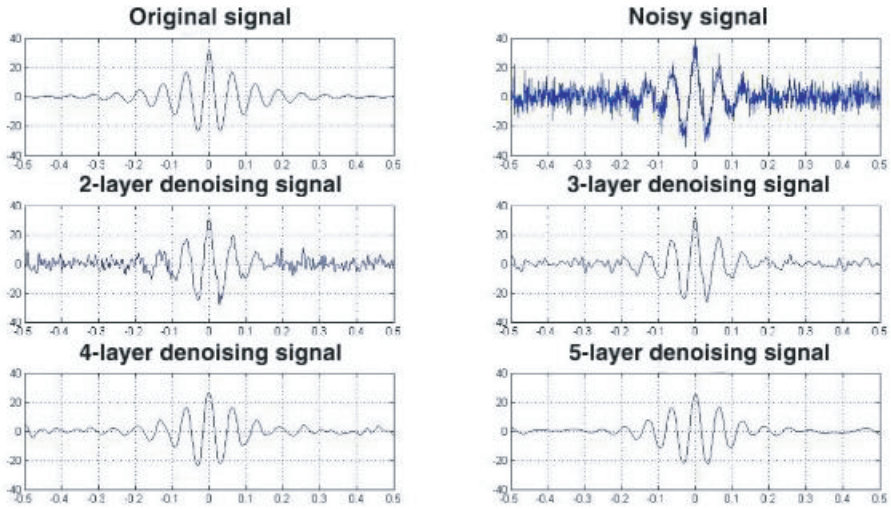

Figure 5. Noise reduction of db6 wavelet.

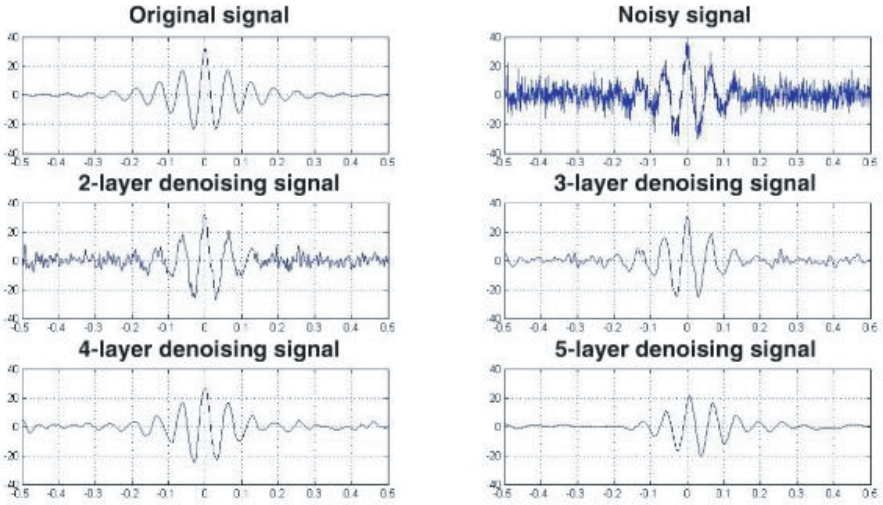

Figure 6. Noise reduction of sym4 wavelet db6.

Table 2. Evaluation of the noise reduction effect with different wavelet bases and decomposition layers.

Base	$N=2$		$N=3$		$N=4$		$N=5$	
	SNR	RMSE	SNR	RMSE	SNR	RMSE	SNR	RMSE
haar	7.1171	3.1534	8.3999	2.7211	6.0999	3.5461	−0.0490	7.1977
db4	7.3349	3.0761	10.148	2.2252	11.149	1.9828	0.3036	6.9113
db6	7.5584	2.9980	10.128	2.2301	11.873	1.8242	12.609	1.6761
sym4	7.3925	3.0558	10.119	2.2325	11.368	1.9335	3.8977	4.5694
sym6	7.5095	3.0149	10.132	2.229	11.927	1.8130	3.6998	4.6747
coif2	7.3307	3.0776	10.137	2.2279	11.345	1.9386	3.6050	4.7260
coif4	3.3532	3.0696	10.180	2.2168	11.992	1.7994	0.1569	7.0290
bior3.9	7.3718	3.0630	10.081	2.2422	11.980	1.8020	3.7071	4.6708
bior6.8	7.5548	2.9992	10.102	2.2370	11.929	1.8125	2.5303	5.3484
rbio3.7	7.3956	3.0546	9.9841	2.2675	10.821	2.0591	1.844	5.7882
rbio6.8	7.5335	3.0064	10.144	2.2260	11.887	1.8214	2.4424	5.4028

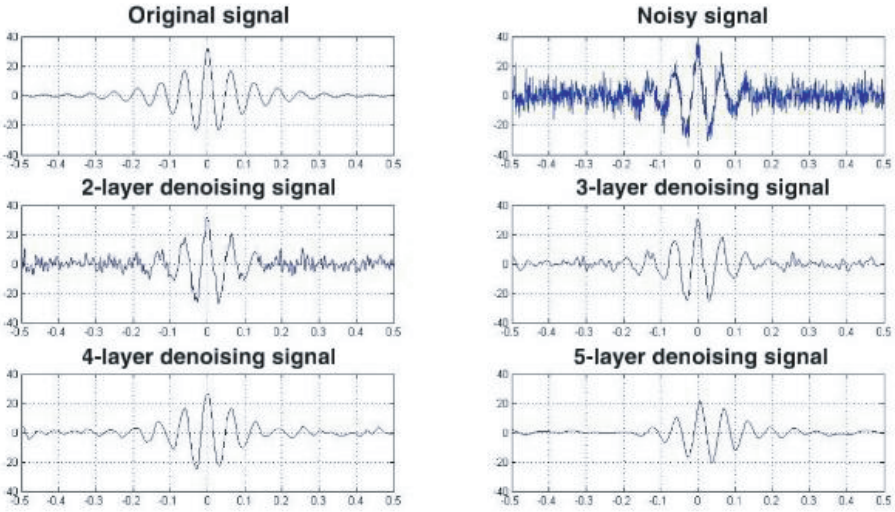

Figure 7. Noise reduction of sym6 wavelets.

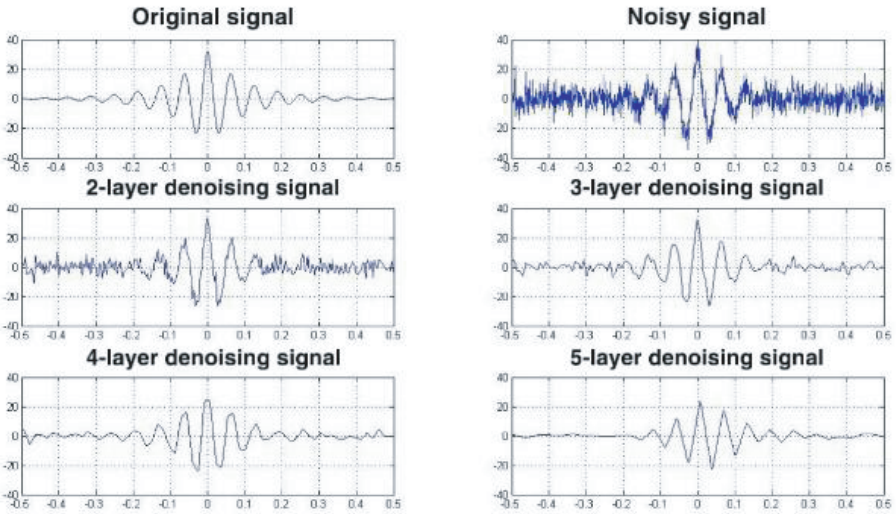

Figure 8. Noise reduction of coif2 wavelets sym6.

signal, the number of decomposition layers N is chosen as 3 or 4. Considering that the subsequent spin-echo signal processing is more concerned with the amplitude decay characteristics, N should be taken as 3 to reduce the distortion.

In addition, comparing the decomposition of different wavelet bases, we can see that the haar wavelet has the worst noise reduction effect, and the reconstructed signal is discontinuous, which is caused by the discontinuity of the haar wavelet itself. The wavelets other than the haar wavelet have good continuity and good similarity to the spin-echo signal so that the signal-to-noise ratio can reach around 10 at $N = 3$.

Among them, the dbN wavelet system, coifN wavelet system, and symN wavelet system are wavelets constructed by Daubechies. dbN wavelets have good continuity but are not symmetric; symN wavelets are an improvement of dbN wavelets; coifN wavelets have better symmetry than dbN. In terms of support length, coifN has the same support length as db3N and sym3N; in terms of the number of vanishing moments, coifN has the same number of vanishing moments as sym2N [29]. While bior and rbio are double orthogonal spline wavelets and inverse double orthogonal spline wavelets respectively, compared

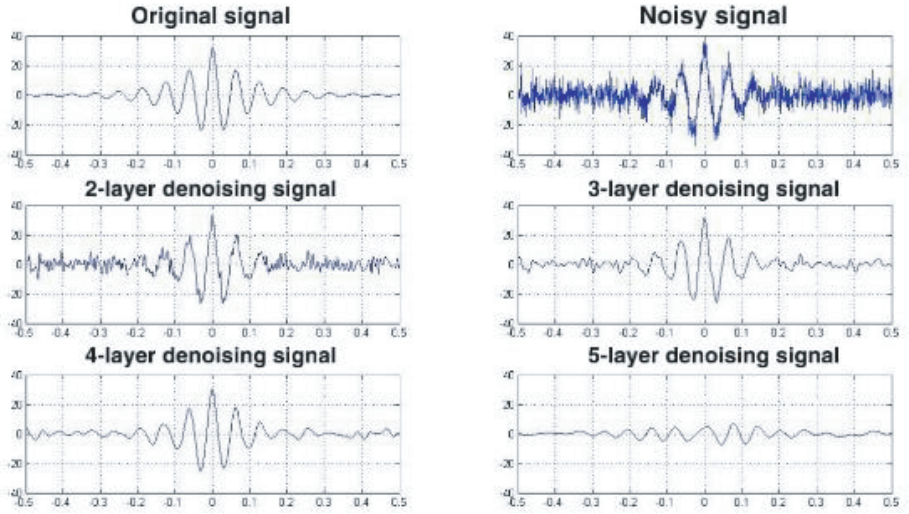

Figure 9. Noise reduction of coif4 wavelets.

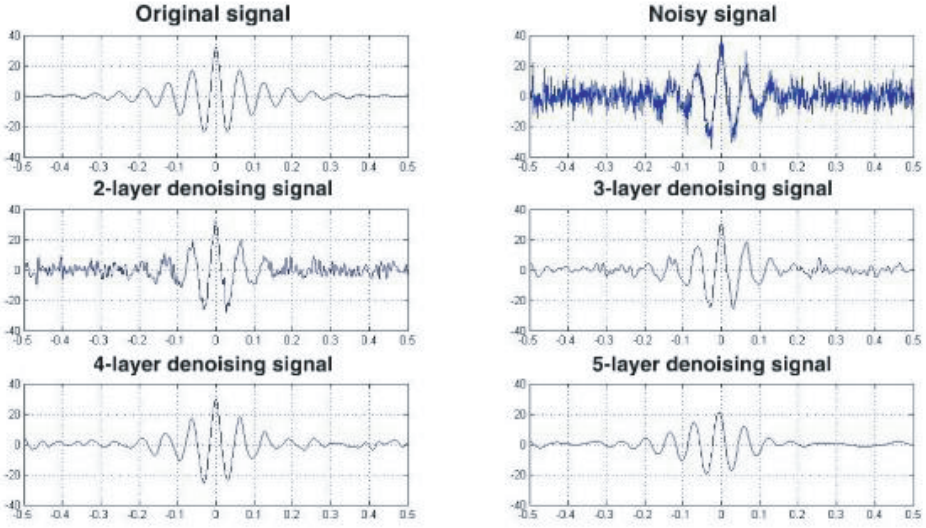

Figure 10. Noise reduction of bior3.9 wavelets.

to Daubechies and haar wavelets, the spline wavelets are not only continuous but also symmetric and have good properties.

4.2. Noise Reduction with Different Thresholds

The previous subsection compares the noise reduction effects under different wavelet bases and decomposition layers and concludes that the noise reduction effect is most suitable for $N = 3$. In the following section, a more representative sample wavelet bior3.9 and an approximate symmetric wavelet coif4 constructed by Daubechies are selected for comparative analysis of thresholding, which is implemented here using Matlab's wavelet tools menu wavemenu.

It should be noted that since the threshold ranges obtained using different wavelet base decompositions are different, the threshold processing is uniformly expressed in percentage form for the sake of comparative analysis, and the threshold T is the percentage of the set threshold in the

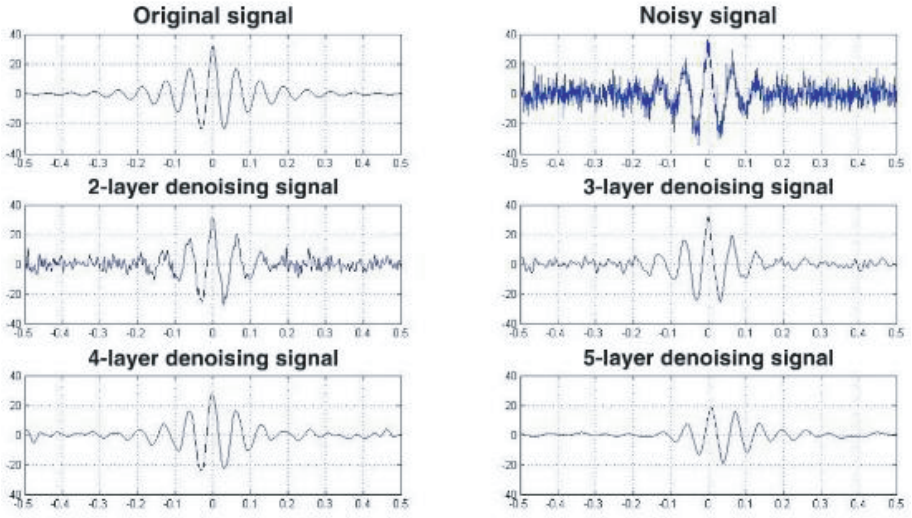

Figure 11. Noise reduction of bior6.8 wavelets.

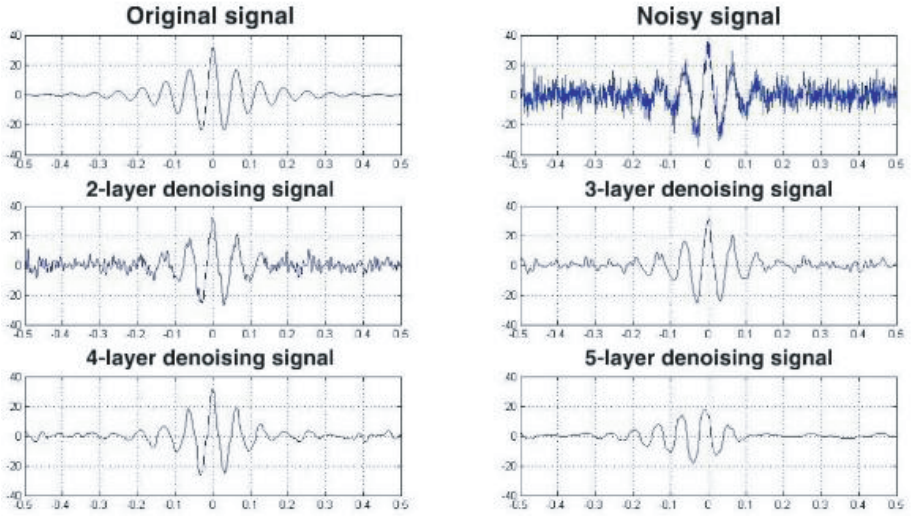

Figure 12. Noise reduction of rbio3.7 wavelets.

Table 3. Comparison of noise reduction thresholds using coif4 wavelet bases ($N = 3$).

Method	$T = 15\%$		$T = 30\%$		$T = 50\%$		$T = 70\%$		$T = 85\%$	
	SNR	RMSE	SNR	RMSE	SNR	RMSE	SNR	RMSE	SNR	RMSE
Soft	3.839	5.405	8.256	2.767	9.783	2.321	10.34	2.176	10.49	2.138
Hard	2.312	5.485	3.580	4.740	5.793	3.674	7.767	2.927	9.447	2.412

maximum value of wavelet coefficients at that level.

Table 3 gives the results of the threshold treatment using coif4 for the $N = 3$ condition.

Table 4 gives the results of the threshold treatment using bior3.9 for the $N = 3$ condition.

The soft thresholding method is more effective than the hard thresholding method in terms of noise reduction, and its noise reduction quality improves as the threshold increases, but as can be seen from

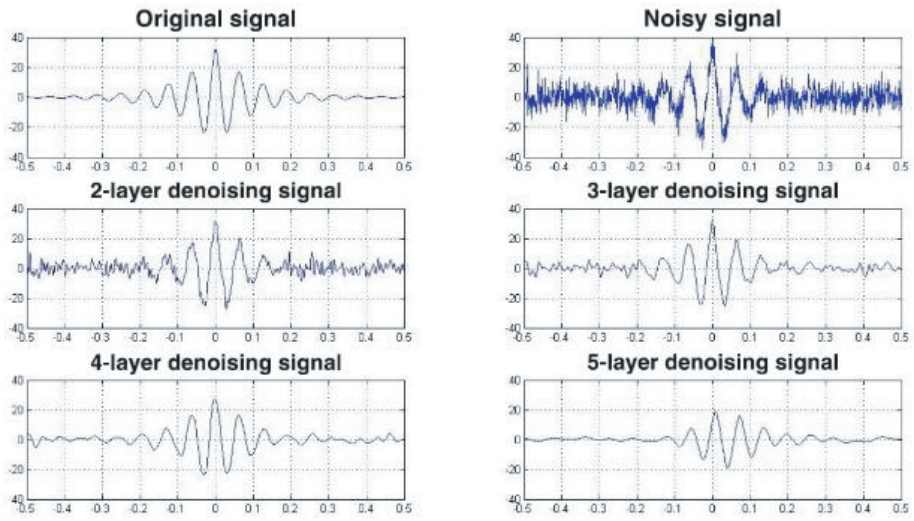

Figure 13. Noise reduction of rbio6.8 wavelets.

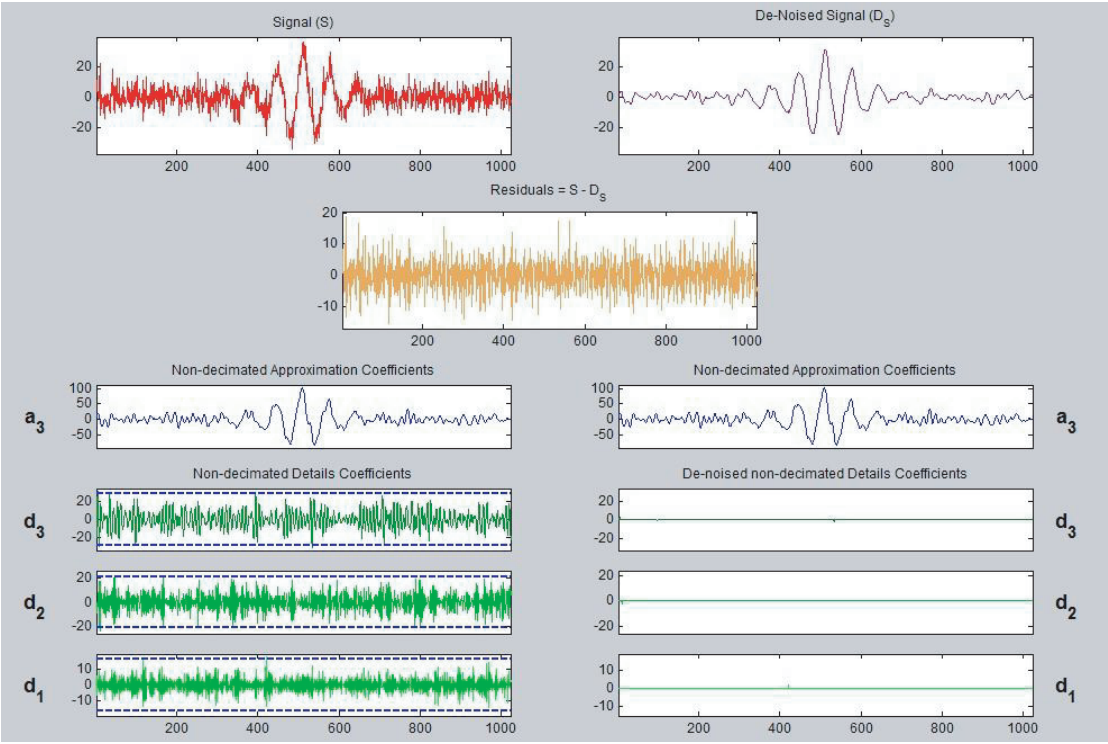

Figure 14. Bior3.9 soft threshold denoising process ($N = 3$, $T = 0.9$).

the data in Table 2 ($T = 100\%$), its optimal threshold value occurs between 85% and 100%, not the larger the better.

Comparing the noise reduction effects of bior3.9 wavelet and coif4 wavelet under the same threshold, it is found that the noise reduction effect of the spline wavelet is better, which is caused by the excellent nature of the spline wavelet in terms of symmetry and continuity, and therefore, the spline wavelet is widely used. Figure 14 gives the whole noise reduction process when bior3.9 is chosen as the wavelet base, N taken as 3, and T taken as 90% soft threshold. At this point SNR = 10.5749, RMSE = 2.1184.

Table 4. Comparison of noise reduction thresholds using bior3.9 wavelet bases ($N = 3$).

Method	$T = 15\%$		$T = 30\%$		$T = 50\%$		$T = 70\%$		$T = 85\%$	
	SNR	RMSE	SNR	RMSE	SNR	RMSE	SNR	RMSE	SNR	RMSE
Soft	5.320	3.879	7.988	2.853	9.911	2.287	10.48	2.141	10.57	2.121
Hard	2.315	5.483	3.500	4.784	5.713	3.707	8.308	2.750	10.02	2.257

5. CONCLUSION

In this paper, by building a simulation model of the spin-echo signal measured by a single-sided NMR sensor, wavelet analysis is used to realize the noise reduction processing of the spin-echo signal containing noise, and the effects of wavelet basis, decomposition level, and threshold selection on the noise reduction effect are discussed with the signal-to-noise ratio SNR and mean square error RMSE as evaluation indexes respectively. The simulation results show that the introduction of wavelet noise reduction technique into the processing of single-sided NMR measurement signals can greatly improve the signal quality, which is of great significance to improve the later data analysis of single-sided NMR.

The use of wavelet analysis for signal denoising is a complex process. In this paper, a simplified spin-echo signal is used as a simulation signal to explore and demonstrate the feasibility of wavelet analysis for denoising single-sided NMR spin-echo signals. For the real one-sided NMR spin-echo signal, more and more complicated problems will be involved, and the optimal noise reduction solution for the one-sided NMR spin-echo signal can only be found by considering the characteristics of the wavelet basis and the signal characteristics, as well as the influence of the number of decomposition layers and the choice of the threshold value.

ACKNOWLEDGMENT

This research was funded by the National Natural Science Foundation of China (No. 51707028), and Science and Technology Funds of Chongqing Municipal Education Commission (KJQN202100533).

REFERENCES

1. Blumich, B., J. Perlo, and F. Casanova, "Mobile single-sided NMR," *Progress in Nuclear Magnetic Resonance Spectroscopy*, Vol. 52, 197–269, 2008.
2. Goga, N. O., A. Pirnau, L. Szabo, et al., "Mobile NMR: Applications to materials and biomedicine," *Journal of Optoelectronics and Advanced Materials*, Vol. 8, No. 4, 1430, 2006.
3. Blümich, B., F. Casanova, J. Perlo, et al., "Advances of unilateral mobile NMR in nondestructive materials testing," *Magnetic Resonance Imaging*, Vol. 23, No. 2, 197–201, 2005.
4. Blümich, B., "Applications in biology and medicine," *Single-Sided NMR*, 187–202, Springer, Berlin, Heidelberg, 2011.
5. Xia, Y., Z. Xu, J. Huang, J. Lin, and D. Yu, "Unilateral mini NMR sensor used for assessing the aging status of the sheds of composite insulators," *Progress In Electromagnetics Research M*, Vol. 42, 145–152, 2015.
6. Xu, Z., L. Li, P. Guo, et al., "Portable unilateral NMR measuring system for assessing the aging status of silicon rubber insulators," *Applied Magnetic Resonance*, Vol. 50, No. 1, 277–291, 2019.
7. Abragam, A., *Principles of Nuclear Magnetism*, Oxford University Press, Oxford, 1983.
8. Hansen, P. C., "Analysis of discrete ill-posed problems by means of the L-curve," *SIAM Review*, Vol. 34, No. 4, 561–580, 1992.
9. Ross, M. M. B., G. R. Wilbur, P. F. de J. Cano Barrita, and B. J. Balcom, "A portable, submersible, MR sensor — The Proteus magnet," *Journal of Magnetic Resonance*, Vol. 326, 1–8, 2021.

10. Guoxing, X. and L. Liben, *Principles of Nuclear Magnetic Resonance Imaging (in Chinese)*, Science Press, 2007.
11. Wang, F., L. Miao, S. Wang, et al., "Application of improved wavelet denoising method in GPS attitude determination," *Journal of Astronautics*, Vol. 29, No. 4, 1267–1271, 2008.
12. Gao, Z., L. Hua, H. Zheng, et al., "Physicochemical characteristics of fly ashes and situation & prospect of its utilization as resources," *Journal of Capital Normal University*, Vol. 24, No. 1, 50–54, 2003.
13. Mohan, J., V. Krishnaveni, and Y. Guo, "A survey on the magnetic resonance image denoising methods," *Biomedical Signal Processing and Control*, Vol. 9, 56–69, 2014.
14. Gerig, G. and O. Kubler, "Nonlinear anisotropic filtering of MRI data," *IEEE Transactions on Medical Imaging*, Vol. 11, No. 2, 221–232, 1992.
15. Krissian, K. and S. Aja-Fernandez, "Noise-driven anisotropic diffusion filtering of MRI," *IEEE Transactions on Image Processing*, Vol. 18, No. 10, 2265, A Publication of the IEEE Signal Processing Society, 2009.
16. Pizurica, A., W. Philips, I. Lemahieu, and M. Acheroy, "A versatile wavelet domain noise filtration technique for medical imaging," *IEEE Transactions on Medical Imaging*, Vol. 22, 323–331, 2003.
17. Muresan, D. D. and T. W. Parks, "Adaptive principal components and image denoising," *IEEE International Conference on Image Process*, Vol. 1, 101–104, 2003.
18. Yaroslavsky, L. P., K. Egiazarian, and J. Astola, "Transform domain image restoration methods: Review, comparison and interpretation," *Nonlinear Image Processing and Pattern Analysis XII*, Vol. 4304, 155–169, 2000.
19. Awate, S. P. and R. T. Whitaker, "Nonparametric neighborhood statistics for MRI denoising," *International Conference on Information Processing in Medical Imaging*, Springer-Verlag, 2005.
20. Manjón, J. V., P. Coupé, A. Buades, D. Louis Collins, and M. Robles, "New methods for MRI denoising based on sparseness and self-similarity," *Medical Image Analysis*, Vol. 16, No. 1, 18–27, 2012.
21. Zhang, K., W. Zuo, Y. Chen, et al., "Beyond a Gaussian denoiser: Residual learning of deep CNN for image denoising," *IEEE Transactions on Image Processing*, Vol. 26, No. 7, 3142–3155, 2016.
22. Jiang, D., W. Dou, L. Vosters, et al., "Denoising of 3D magnetic resonance images with multi-channel residual learning of convolutional neural network," *Japanese Journal of Radiology*, Vol. 36, 566–574, 2018.
23. Gang, C., "Research on the application of MRI image denoising methods in Chinese)," *The Medical Forum*, 2019.
24. Torrence, C. and G. P. Compo, "A practical guide to wavelet analysis," *Bulletin of the American Meteorological Society*, Vol. 79, No. 1, 61–78, 1998.
25. Coifman, R. R., Y. Meyer, and V. Wickerhauser, "Wavelet analysis and signal processing," *Wavelets and Their Applications*, 1992.
26. Walnut, D. F., *An Introduction to Wavelet Analysis*, Springer Science & Business Media, 2002.
27. Mingcai, L., *Wavelet Analysis and Its Applications*, 1, Tsinghua University Press, Beijing, 2005.
28. Pan, G., "Research on key technology and applications of portable and fully open magnetic resonance instrument," Chongqing University, 2015.
29. Tang, L. W. and D. F. Tang, "Wavelet signal denoising technique based on matlab," *Journal of Hunan University of Science & Technology*, Vol. 29, No. 1, 85–87, 2014.
30. O'Reilly, T. and A. G. Webb, "In vivo T1 and T2 relaxation time maps of brain tissue, skeletal muscle, and lipid measured in healthy volunteers at 50 mT," *Magnetic Resonance in Medicine*, Vol. 87, No. 2, 884–895, 2022.